This is an *Accepted Manuscript*, which has been through the Royal Society of Chemistry peer review process and has been accepted for publication.

Accepted Manuscripts are published online shortly after acceptance, before technical editing, formatting and proof reading. Using this free service, authors can make their results available to the community, in citable form, before we publish the edited article. We will replace this *Accepted Manuscript* with the edited and formatted *Advance Article* as soon as it is available.

You can find more information about *Accepted Manuscripts* in the **Information for Authors**.

Journal Name

COMMUNICATION

High-yield halide-free synthesis of biocompatible Au nanoplates

Guoqing Wang,[abc] Shengyang Tao,[ad] Yiding Liu,[a] Lei Guo,[a] Guohui Qin,[a] Kuniharu Ijiro,[c] Mizuo Maeda[b] and Yadong Yin*[a]

We commounicate an unconventional synthesis of Au nanoplates with high yield and excellent reproducibility through polyvinylpyrrolidone (PVP)-assisted H_2O_2 reduction. Unlike the ones prepared using halide-based surfactants, the PVP-capped Au nanoplates are found to afford fairly easy bio-functionalization, suggesting vastly expanded spectrum of application in bio-related fields.

Development of novel synthesis for noble metal (e.g. Au and Ag) nanostructures has been recognized as one of the major enablers for their broad applications in fields ranging from sensing and biotherapy to catalysis and electronics.[1] For instance, Au nanospheres have been routinely used as colorimetric indicators for recognition events based upon their localized surface plasmon resonance (LSPR) properties. [2] Recently, research interests in LSPR have silently shifted to anisotropic metal nanostructures, which exhibit more sensitive optical response to the changes in their own morphologies and local dielectric environment.[3] Of the many anisotropic nanoparticles, Au and Ag nanoplates (e.g., nanotriangles, nanohexagon) with the lateral dimensions significantly larger than their thicknesses are of particular interest.[4] With clear theoretical understanding of the LSPR modes of Ag and Au nanoplates,[5] researchers have applied the attractive LSPR feature for high performance biosensing.[6] For detections based on surface-enhanced Raman scattering (SERS), although Ag naoplates are in principle preferred substrates, Au nanoplates have the advantage of higher chemical stability.[7] Currently, people have further evolved to employ Au nanoplates for expanded applications in bio-related fields. However, it has remained an open challenge for materials chemists to produce Au nanoplates in high quality found in their Ag counterparts. As is accepted so far, the most popular preparation

methods usually afford Au nanoplates in yields below 30–40%, and are strictly dependent on the use of cetyltrimethylammonium (CTA) halide (e.g., bromide, chloride) as the structure-directing capping agent,[7-10] whose toxicity has been of concern to the nanomedicine community.[11,12] Despite the great progress in high-yield synthesis of Au nanotriangles made by Zhang *et al.*,[13] available triangle size was limited to a relatively narrow range (45-120 nm). An additional problem in such synthetic system is that the yield and quality of Au nanoplates are extremely sensitive to the impurity in the capping ligands: it has been discovered that a trace amount of iodide is playing a determining role in directing nanoplate growth, thus bringing a significant problem in reproducibility as the exact amount of iodine impurity in commercial capping ligands could not be controlled.[10] An even greater challenge is met at the usage stage: it has been found to be extremely challenging to replace the CTAB ligands on the Au surface with the desired functional ligands, therefore greatly compromising the potential of those Au nanoplates in an array of applications.[11]

As has been recognized, H_2O_2 plays an interesting and critical role in the synthesis of high quality Ag nanoplates.[14] In those works, H_2O_2 was used as a "magic" reagent thought to help form planar twinned seeds and, meanwhile remove non-twinned particles, finally contributing to produce pure Ag nanoplates. Taking these into account, we deemed it of great curiosity to test if H_2O_2 would promote the growth of Au nanoplates in a way similar to the Ag case. In a typical synthesis, 1 mL of $HAuCl_4$ (10 mM) and 0.2 mL of trisodium citrate (10 mM) were mixed with 18.5 mL of ultra-pure water. Immediately after the addition of 0.5 mL of $NaBH_4$ (0.1 M) under vigorous stirring (800 rpm), the color of the pale yellow solution turned to red, and then orange within a few seconds. Stirring was stopped after reaction for 5 min. The resulting solution was left for aging for over 3 hrs without any disturbance, and then stored as the seeds at 4 °C for future use (see the TEM images of the seed in Fig. S1). In the growth step, 1 mL of $HAuCl_4$ (10 mM) and 2 mL of PVP (2 mM, M.W. 40000) were introduced into 19 mL of ultra-pure water, after which 200 μL of the seed solution was injected. Finally, H_2O_2 (30 wt%) was added to trigger seeded growth of Au nanoplates. The mixture was reacted at room temperature for 3 hr when the volume of H_2O_2 is equal to or more than 5 μL; while the reaction was left overnight if less than 5 μL of H_2O_2 was added.

a. *Department of Chemistry, University of California, Riverside, California 92521, United States.*
b. *Bioengineering Laboratory, RIKEN, 2-1 Hirosawa, Wako-shi, Saitama 351-0198, Japan.*
c. *Research Institute for Electronic Science, Hokkaido University, Kita21, Nishi10, Kita-Ku, Sapporo 001-0021, Japan.*
d. *Department of Chemistry, Dalian University of Technology, Dalian 116024, China*
† Footnotes relating to the title and/or authors should appear here.
Electronic Supplementary Information (ESI) available: additional characterization data, statistics and simulation results. See DOI: 10.1039/x0xx00000x

To investigate the effect of H_2O_2, we carried out a series of parallel syntheses using different amounts of H_2O_2 in the range of 2–90 μL. The extinction spectra of the resultant colloidal particles (without cleaning by centrifugation) in Fig. 1 clearly display well developed bands at wavelengths much longer than the intrinsic LSPR band (~520 nm) for spherical Au nanoparticles, suggesting the development of anisotropic shapes. To look into the morphologies of the products, the resultant reaction solutions were subjected to transmission electron microscopy (TEM) analysis after removal of excess PVP by two-cycle centrifugation (8000 and 7500 rpm for 3 min, respectively) and redispersion, during which some particles may be removed as well. As can be seen in Fig. 2a-d, the TEM images revealed the presence of nanoplate structures of triangular and hexagonal shapes as well as some spheres. The high intensity of the optical bands at longer wavelengths relative to that for nanospheres are indicative of relatively high yield of Au nanoplates, in comparison to those in previous reports.[7-9] The presence of LSPR bands in the infrared (IR)-to-near infrared (NIR) region are attributable to the in-plane dipolar resonance of Au nanoplates.[5] A broad dipolar resonance band was found for the plates synthesized in the presence of 2 μL of H_2O_2, reflecting a wide size distribution. While with the increase in the volume of H_2O_2, the in-plane dipolar resonance band of Au nanoplates blue shifted (Fig. 1), indicating the reduction of aspect ratio. We supposed that the co-existence of nanotriangle and nanohexagon was responsible for the split of the infrared absorption bands of the smaller Au nanoplates, which were obtained with 30 μL of H_2O_2 or more. Over 200 plates were studied for size statistics of each sample, in which the length of edge and diagonal represented the size of triangle and hexagon, respectively. The size of the Au nanoplates was observed to gradually decrease and exhibit narrower distribution with increasing volume of H_2O_2 (Fig. 2e&S2). Up to 90 μL of H_2O_2, the resultant Au nanoplates were as small as ~72 nm (Fig. S3). For larger Au nanoplates, their purity could be greatly improved via centrifugation as supported by the corresponding extinction spectra show in Fig. S4. Furthermore, the mean size of Au nanoplates produced here was able to be readily tuned in the range of 70–510 nm through the choice of H_2O_2 volume in the range 2–90 μL (Fig. 2g).
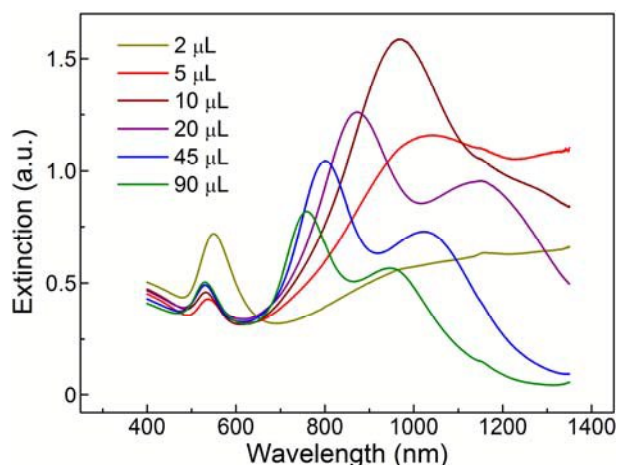
Fig. 1 UV-Vis-NIR spectra of the Au nanoplates dispersions obtained in the presence of different amounts of H_2O_2. Samples directly from syntheses were analyzed without additional purification.
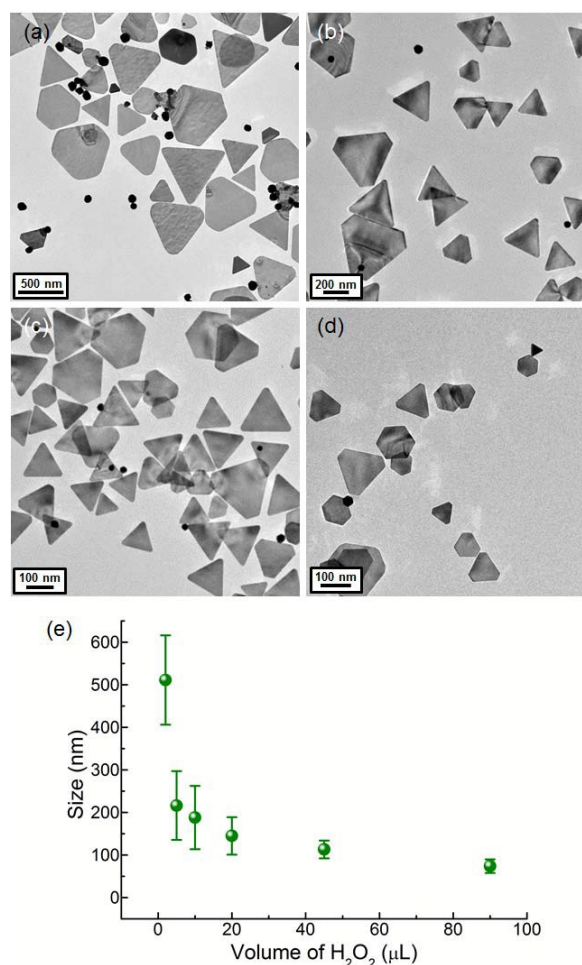
Fig. 2 a-f) Typical TEM images of Au nanoplates obtained in the presence of 2 μL (a), 5 μL (b), 10 μL (c), 20 μL (d) of H_2O_2, respectively. Prior to TEM measurements, products were centrifuged twice to remove excess PVP. Some spheres might be also removed during the process, but no further intentional purification was applied to the samples. (e) Plots of mean size of Au nanoplate against volume of H_2O_2 used. The error bars indicate standard deviations.

The Au nanoplates produced with 5 μL of H_2O_2 served as the model for evaluation of synthetic yield. All colloidal particles were precipitated by centrifugation (10000 rpm, 30 min) to remove excess PVP to better TEM observation. Assuming that each particle was grown from a seed, the yield of nanoplate could be determined to be ~63% by simply calculating the number ratio (Fig. S5a). During our experiments, we further found that heavy Au nanoplates in the products preferentially undergo gravitational sedimentation in 2 days, giving rise to a purity of ~95% without any treatment (Fig. S5b). We calculated the proportion of triangle in plate to be 82.1% after twice centrifugation/washing (Fig. S6). Statistic size measurements (88 triangles studied) showed that the Au nanotriangles produced with 5 μL of H_2O_2 to be ~198.5 nm in average edge length (Fig. S7). The thickness of the Au nanoplates could also be estimated by TEM imaging. When a concentrated sample of the Au nanoplates were deposited on a TEM grid, it was always possible to observe some of them standing vertically upon their edge. Their thickness of the plate was observed to be ~10 nm by using this method (Fig. S8). More accurate measurement of the

plate thickness could be obtained by using atomic force microscopy (AFM). As shown in Fig. 3 and Fig S9, the flat-lying Au nanoplates are uniformly ~12 nm-thick, similar to the value estimated from the standing Au nanoplates by TEM. Survey over 40 nanoplates by AFM further suggested an average thickness of 12.2 nm with a distribution between 10 nm and 15 nm, resulting in an aspect ratio of ~44. Finite-difference time-domain (FDTD) simulations showed that a Au nanotriangle of 198.5 nm in edge length and 12.2 nm in thickness exhibits a dipolar resonance peak at 1052 nm (Fig. S10), which is in good agreement with the experiment result (1044 nm).

PVP was found to play an important role in limiting the growth of the nanoplates along the face direction. It is reasonable to infer that PVP may selectively bind to the two faces and limit the increase of the plate thickness, in a role similar to citrate plays in directing the growth of Ag nanoplates. However, control experiments have revealed that the in-plane dipolar resonance peak gradually blue shifted when more PVP was added to the reaction under otherwise identical conditions (Fig. S11), suggesting its limited selectivity in binding to different facets and promoting the anisotropic growth of the nanoplates. We also found out that when some other typically used capping ligands such as sodium dodecyl sulfate (SDS) and poly(ethylene glycol)-b-poly(propylene glycol)-b-poly(ethylene glycol) (e.g. Pluronic® F-127 and P-123), were used in place of PVP in the synthesis, nanoplates could still form as indicated by UV-Vis spectroscopic analysis. Interestingly, replacing PVP with sodium citrate, which is considered the magic capping ligand that can effectively direct the lateral growth of silver nanoplates, always led to completely spherical particles. All these observations suggest that the ligand-metal interaction and therefore the growth behavior of the plates are very different for these two metals.

The exact mechanism involved in the formation of the Au nanoplates is not yet accessible with our available characterization tools, although one can clearly see the critical role that H_2O_2 is playing in the current synthesis. In the previously reported thermal synthesis of Ag nanoplates, H_2O_2 was found to serve as both an oxidant and a reductant as the reaction was occurring at relatively high pH conditions.[15] It is generally regarded as a powerful oxidizer in acidic solutions, with the standard reduction potential being +0.695 V for the half reaction $(1/2)O_2 + H_2O + e \rightarrow H_2O_2$. Due to the high redox potential of Au(III) (+1.5 V),[16] however, in this case H_2O_2 mainly acts as a reductant that reduces Au(III) to metallic Au for supporting the growth of Au plates.
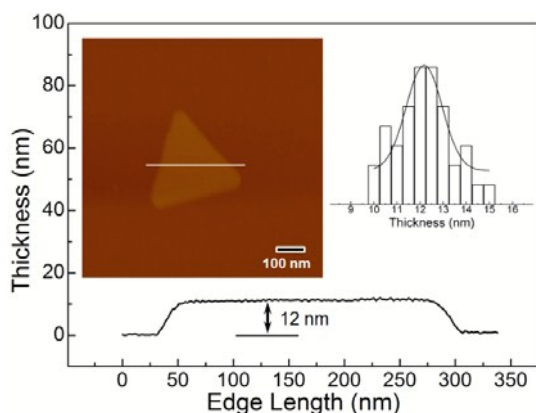
Fig. 3 A representative AFM image and the corresponding height profile of a Au nanoplate synthesized in the presence of 5 μL of H_2O_2 and its. The insert histogram shows the thickness distribution of the Au nanoplates studied.

While it has been assumed that the oxidative nature of H_2O_2 caused the formation of twin defects in Ag seeds which further grew into plates, the Au seeds in the current work were produced in the absence of H_2O_2. Although the preformed seeds are needed in the current synthesis, the growth might not be a simple seed-mediated process, as indicated by the fact that more H_2O_2 did not produce larger plates. In fact, we observed that when there were no seeds present, the reduction of Au(III) by H_2O_2 proceeded very slowly, with no appreciable changes to the solution after 6 hours. In contrast, in the presence of Au seeds, noticeable changes to the color of the solution could be observed within 5 minutes, indicating the quicker occurrence of the reduction reaction. This observation may lead to the conjecture that the metallic Au seeds may serve as the catalysts for initiating the decomposition of H_2O_2 and subsequently promoting the reduction reaction of the Au cations. However, we have observed no sign of gas release by aging a mixture of seed solution and H_2O_2 for 3 hours, indicating no catalytic decomposition of H_2O_2 in the presence of Au seeds. The aged mixture remained active and could be used for the subsequent growth if gold precursor was added, producing nanoplates in a way very similar to the case without aging. With all these evidences, it is reasonable to conclude that in this case, the Au seeds may play their basic role in promoting the growth reaction by reducing the energy barrier of the precipitation of reduced Au species.

We believe the higher stability of Au than Ag against oxidative etching is the major cause of the different growth behaviors of their corresponding nanoplates. In the case of Ag, the oxidative etching dissolves the initially formed Ag seeds and only leaves more stable twinned seeds for further growth into nanoplates. While in the case of Au, we did not observe clearly the steps of seed dissolution and regrowth, it is still possible that the oxidative etching by H_2O_2 may cause changes in the crystal structures of the seeds so that lateral growth becomes favored. More systematic studies of the reaction and more detailed microscopic analysis of the structures of the seeds and nanoplates are required to reveal the mechanism involved in the current synthesis of Au nanoplates.

Since the bottleneck for the application of conventional Au nanoplates lies in the high toxicity of the CTA-composed bilayers and the difficulty in surface modification, the PVP-capped Au nanoplates have their advantages in biocompatibility. As PVP is an approved chemical by the U.S. Food and Drug Administration (FDA), we demonstrate here the easiness of the surface modification of the PVP-capped nanoplates by using the sample prepared using 5 μL of H_2O_2. DNA modification of the Au nanoplates were conducted by simple addition of DNA1 (HS-5'-TAC TCC TTA TTA CGC CAC CAG CTC C-3') and incubation for 3 hours, followed by centrifugation to remove excess DNA and re-dispersion in PB buffer (10 mM, pH 7.3) (Fig. 4a). The surface of the Au nanoplates after DNA treatment was analyzed to be more negatively charged (-24.7 mV) than that before (-19.6 mV), validating the success of DNA attachment. Under the identical condition, in contrast, DNA addition to the CTA chloride-capped Au nanoplates (with a zeta potential of 10.6 mV) induced formation of irreversible aggregates due to the electrostatic interaction (Fig. S12), which has been frequently observed for their nanorod counterparts.[11]

In order to confirm the binding of DNA on the Au nanoplates, Au nanospheres (15 nm in diameter) modified with DNA2 (HS-5'-

COMMUNICATION

Journal Name

TTT TTT TTT GGA GCT GGT GGC GTA A-3') that can hybridize to DNA1 were introduced to the DNA-modified Au nanoplates at different mixing ratios.[17] After incubation for 3 hours in the presence of NaCl (50 mM), large aggregates can be directly observed in the solution. The mixtures were then subjected to TEM analysis without purification. Formation of hetero-assemblies was subsequently validated. Remarkably, we noticed that the Au nanoparticles preferentially attached to the nanoplate edges, other than the top/bottom surfaces (Fig. S13 a-c). The results may be attributed by the high DNA density on the edge region that originates from the crystalline structure or higher curvature for DNA loading, a consequence similar to the prior ligand exchange on the end regions for gold nanorod.[18] With increasing amount of DNA-modified Au nanoparticles, more Au nanoparticles were brought to both the edges and the flat top/bottom surfaces, suggesting controllable assembly by DNA hybridization. According to our TEM observation, free nanoparticles hardly existed throughout all the mixing ratios studied here (Fig. S13d-f). This implied the large surfaces of the Au nanoplates were still unsaturated for accommodating Au nanoparticles. Up to the ratio of the nanoparticles at 50 relative to the nanoplates, we discovered the formation of DNA-crosslinked large hetero-assemblies of the Au nanoplates and the Au nanoparticles. Indeed, this result was not unexpected since the increase in the number of multivalent Au nanoparticles would promote the crosslinking of Au nanoplates and bring about sandwiched plate-particle-plate nanostructures. As a control, the DNA2-modified Au nanoparticles and unmodified Au nanoplates were mixed under the identical condition. No apparent aggregation can be visually observed. Characterization by TEM did not show sandwiched hetero-assemblies, despite of some non-specific adsorption (Fig. 4b). The stacking of Au nanoplates shown in Fig. 4b was due to the strong capillary force during the drying process. This is typical for plate-like nanostructures, especially when the solution is high in ionic strength (Fig. 4b) or nanoplate concentration (Fig. S8).

The hetero-assemblies made by DNA crosslinking were then subjected to SERS detection, in which a non-charged analyte molecule, 2,2'-dithiodipyridine (DTDP, 1.0×10^{-5} M) acted as the analyte (Fig. S14). The plate-particle simple mixture showed the SERS intensity similar to that of the Au nanoplates, indicating the dominant role of the Au nanoplates in the contribution to Raman signal enhancement. This dominance has indeed been reported for the Ag nanoparticle and nanoplate assemblies.[19] The DNA-induced assemblies of Au nanoplates and nanoparticles were found to afford much stronger Raman signal, in comparison to the other two. The enhancement factor was further estimated to be 0.48×10^5, assuming all DTDP molecules were adsorbed on the assemblies. The value was in line with that for a closely packed Au nanotriangle film.[7] More interestingly, well-resolved bands at ~950 cm^{-1} (937 cm^{-1} and 956 cm^{-1}) and 1311 cm^{-1} emerged in the profile, other than the other two, originating from stretching and bending of the C-H bonds, respectively.[20] The enhanced Raman intensity coupled with the finer fingerprint is believed to be a consequence of the induced plasmon coupling between the nanoplates and nanoparticles.
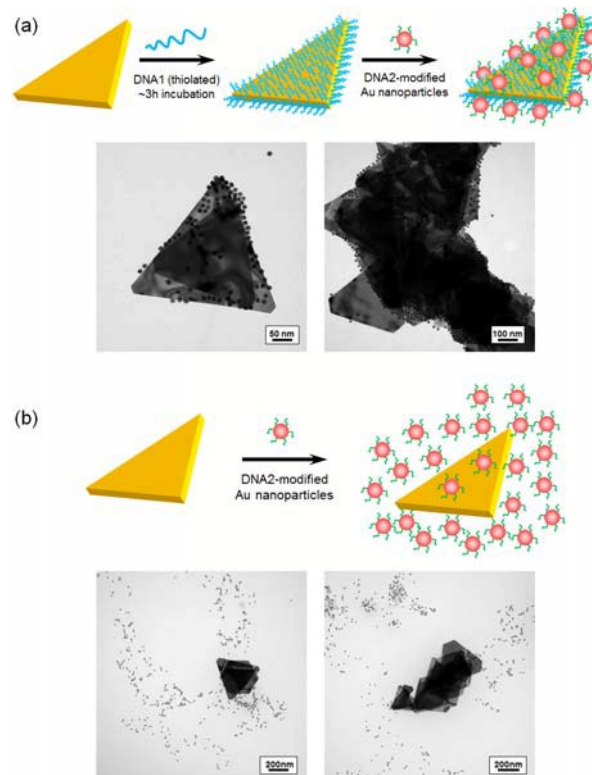
Fig. 4 Schematic representation and TEM characterization for hetero-assembly of DNA2-modified Au nanoparticles and the Au nanoplates with (a) and without DNA1 (b) modification. Nanoparticles and nanoplates were mixed at a ratio of 50 : 1 for both cases.

To sum up, we have described an efficient and robust seeded growth route to biocompatible Au nanoplates through polyvinylpyrrolidone (PVP)-assisted H_2O_2 reduction. Depending on the concentration of H_2O_2, Au nanoplates could be produced in high yield with the lateral dimension fully tunable in the range of 70–510 nm. Unlike the conventional CTA-capped ones associated with cytotoxicity and complicated surface modification, the PVP-capped Au nanoplates possess advantages of biocompatibility and ease of biofunctionalization. As a proof-of-concept, DNA modification of the PVP-capped Au nanoplates was conducted by simple incubation. Highly controllable hetero-assembly of the Au nanoplates and Au nanoparticles clearly indicated DNA attachment onto the nanoplate surfaces, and meanwhile resulted in excellent SERS activity through the induced plasmon coupling. Given the merits of high yield, wide size tuning range and ease of surface modification of the Au nanoplates, the present approach would be urgently needed for the materials community for exploring new applications of such anisotropic nanostructures.

Notes and References

COMMUNICATION

1 J. N. Anker, W. P. Hall, O. Lyandres, N. C. Shah, J. Zhao and R. P. Van Duyne, *Nat. Mater.*, 2008, **7**, 442; N. Rosi and C. A. Mirkin, *Chem. Rev.*, 2005, **105** 1547; G. Wang, H, Tanaka, L. Hong, Y. Matsuo, K. Niikura, M. Abe, K. Matsumoto, T. Ogawa and K. Ijiro, *J. Mater. Chem.*, 2012, **22**, 13691; A. Ruditskiy, S.-I. Choi, H.-C. Peng, and Y. Xia, *MRS Bulletin* 2014, **38**, 335.

2 K. Saha, S. S. Agasti, C. Kim, X. Li and V. M. Rotello*, Chem. Rev.*, 2012, **113**, 2739; G. Wang, Y. Wang, L. Chen and J. Choo, *Biosens. Bioelectron.*, 2010, **25**, 1859.

3 H. J. Chen, X. S. Kou, Z. Yang, W. H. Ni and J. F. Wang, *Langmuir*, 2008, **24**, 5233; G. Wang, Z. Chen, L. Chen, *Nanoscale*, 2011, **3**, 1756; C. J. Murphy, T. K. Sau, A. M. Gole, C. J. Orendorff, J. Cao, L. Gou, S. E. Hunyadi and T. Li, *J. Phys. Chem.*, 2005, **109**, 13875.

4 J. Goebl, Q. Zhang, L. He and Y. Yin, *Angew. Chem. Int. Ed.*, 2012, **51**, 552; J. E. Millstone, S. J. Hurst, G. S. Métraux, J. I. Cutler and C. A. Mirkin, *Small*, 2009, **5**, 646.

5 K. L. Kelly, E. Coronado, L. L. Zhao and G. C. Schatz, *J. Phys. Chem. B*, 2003, **107**, 668; I. Pastoriza-Santos and L. M. Liz-Marzán, *J. Mater. Chem.*, 2008, **18**, 1724.

6 C. Gao, Z. Lu, Y. Liu, Q. Zhang, M. Chi, Q. Cheng and Y. Yin, *Angew. Chem. Int. Ed.*, 2012, **51**, 5629.

7 L. Scarabelli, M. Coronado-Puchau, J. J. Giner-Casares, J. Langer and L. M. Liz-Marzán, *ACS Nano*, 2014, **8**, 5833.

8 L. Bi, Y. Rao, Q. Sun, D. Li, Y. Cheng, J. Dong and W. Qian, *J. Nanosci. Nanotechnol.* 2012, **12**, 4514.

9 J. E. Millistone, G. S. Métraux and C. A. Mirkin, *Adv. Funct. Mater.*, 2006, **16**, 1209.

10 J. E. Millistone, W. Wei, M. R. Jones, H. Yoo and C. A. Mirkin, *Nano Lett.* 2008, **8**, 2526; J. S. DuChene, W. Niu, J. M. Aendroth, Q. Sun, W. Zhao, F. Huo and W. D. Wei, *Chem. Mater.*, 2013, **25**, 1392.

11 I. P. Lau, H. Chen, J. Wang, H. C. Ong, K. C.-F. Leung, H. P. Ho, S. K. Kong, *Nanotoxicology*, 2012, **6**, 847; Q. Dai, J. Coutts, J. Zou and Q. Hou, *Chem. Commun.*, 2008, 2858.

12 A. S. D. S. Indrasekara, R. C. Wadams and L. Fabris, *Part. Part. Syst. Charact.*, 2014, **31**, 819.

13 L. Chen, F. Ji, Y. Xu, L. He, Y. Mi, F. Bao, B. Sun, X. Zhang, and Q. Zhang, *Nano Lett.*, 2014, **14**, 7201.

14 Q. Zhang, N. Li, J. Goebl, Z, Lu and Y. Yin, *J. Am. Chem. Soc.*, 2011, **133**, 18931; N. Li, Q. Zhang, S. Quilivian, J. Goebl, Y. Gan and Y. Yin, *Chem. Phys. Chem.*, 2012, **13**, 2526.

15 T. Parnklang, C. Lertvachirapaiboon, P. Pienpinijtham, K. Wongravee, C. Thammacharoen and S. Ekgasit, *RSC Adv.*, 2013, **3**, 12886; H. Yu, Q. Zhang, H. Liu, M. Dahl, J. B. Joo, N. Li, L. Wang and Y. Yin, *ACS Nano*, 2014, **8**, 10252.

16 *Standard Potentials in Aqueous Solution*, ed. A. J. Bard, R. Parsons and J. Jordan, CRC Press, New York and Basel, 1985.

17 References for DNA modification of Au nanoparticles: K. Sato, K. Hosokawa and M. Maeda, *J. Am. Chem. Soc.*, **2003**, *125*, 8102; K. Sato, K. Hosokawa and M. Maeda, *Nucleic. Acids Res.*, **2005**, *33*, e4.

18 H. Chen, L. Shao, Q. Li AND J. Wang, *Chem. Soc. Rev.*, **2013**, *42*, 2679.

19 J. Zeng, X. Xiao, M. Rycenga, P. Henneghan, Q. Li and Y. Xia, *Angew. Chem. Int. Ed.*, **2011**, *50*, 244.

20 H. I. S. Nogueira, S. M. G. Cruz, P. C. R. Soares-Santos, P. J. A. Ribeiro-Claro and T. Trindade, *J. Raman. Spectrosc.* 2003, 34, 350; H. I. S. Nogueira, P. C. R. Soares-Santos, S. M. G. Cruz and T. Trindade, *J. Mater. Chem.*, **2002**, *12*, 2339.

ChemComm Accepted Manuscript

TOC Graphic: